

<https://doi.org/10.1038/s43247-024-01403-w>

# Anthropogenic eutrophication and stratification strength control hypoxia in the Yangtze Estuary

Check for updates

Hui Sheng<sup>1,2</sup>, Stephen E. Darby<sup>3</sup>, Ning Zhao<sup>2</sup>✉, Dongyan Liu<sup>2</sup>, Albert J. Kettner<sup>4</sup>, Xixi Lu<sup>5</sup>, Yang Yang<sup>6</sup>, Jianhua Gao<sup>1</sup>, Yaqing Zhao<sup>2</sup> & Ya Ping Wang<sup>1,2</sup>✉

Many large estuaries are threatened by intensifying hypoxia. However, due to the limited duration of available observations, uncertainties persist regarding the level of contemporary hypoxia intensity in a longer-term context and the relative contributions of climate versus human factors. Here we present sediment records for the hypoxia intensity and associated environmental parameters in the Yangtze Estuary over the past three centuries. The results show that the hypoxia intensity has been increasing during the last half century due to anthropogenic eutrophication, but the current hypoxia condition is not as severe as some preindustrial periods due to weaker stratification in the water column. Our findings suggest that if anthropogenic and climatic forcing coincide in the foreseeable future, the hypoxia intensity of the Yangtze Estuary may reach unprecedented levels.

Severe oxygen depletion, termed hypoxia (defined as dissolved oxygen (DO) level <2 mg/l), poses a risk to marine life<sup>1,2</sup>. As regions with ecological and economic values, large estuaries are amongst the areas that are most affected by hypoxia hazards<sup>1,3</sup>. Indeed, observations show that the magnitude, frequency and extent of hypoxia outbreaks in many large estuaries have been increasing, and there are growing concerns about the threat that such changes pose to the sustainability of estuarine ecosystems<sup>1,4,5</sup>. The world's large rivers (such as the Mississippi and the Yangtze) deliver large volumes of freshwater and nutrients to their estuaries and shelves, favoring hypoxia by stratification and eutrophication<sup>6,7</sup>. Catchment freshwater and nutrient discharges into those estuaries and shelves are affected by climate (mainly rainfall) and anthropogenic stresses (agriculture, urbanization, etc.)<sup>2,8,9</sup>. Meanwhile, regional hydrological dynamics near river mouths and shelves are modulated by ocean circulation<sup>10,11</sup>. Thus, the risk of hypoxia in the world's large estuaries and shelves is now recognized as being driven by a more complex, but as yet poorly understood, interplay between climate variability and human activities than other coastal or open ocean systems<sup>6,12</sup>.

Scientific progress has been made in our understanding of the patterns, drivers, and consequences of hypoxia, and the potential impacts of human activities on hypoxia in the world's large river estuaries have been reported in a range of studies<sup>1,6,13</sup>. However, only short-term (usually <50 years) and temporally discontinuous monitoring data exist, thus our understanding of

hypoxia events in estuaries is biased toward intervals with heavy anthropogenic influences. Limitations in the duration of observational data, therefore, make it challenging to identify whether current episodes of hypoxia are more severe or frequent than those that occurred prior to human disturbances<sup>14</sup>. This also leads to difficulties in discerning the role of climate variability in driving hypoxia, even though climate is potentially a key vector for developing hypoxia in estuaries<sup>10,15,16</sup>. Here, we address these challenges by using sediment-based proxies to extend the time series of hypoxia and its primary controlling factors to the preindustrial period for an exemplary large estuary, the Yangtze Estuary.

The Yangtze Estuary is a critical zone for land-sea interactions where the freshwater and nutrients supplied by the world's third-largest river interact strongly with oceanographic processes of the East China Sea (Fig. 1). Similar to other large river estuaries, the Yangtze Estuary has been suffering from severe and widespread seasonal hypoxia<sup>6</sup>. Based on observations, some regions of the estuary have experienced hypoxia disasters with extremely high frequency (referred to as hypoxia hot spots) (Fig. 1), and the intensity and frequency of hypoxia hot spots have increased over the past few decades<sup>17,18</sup>. The hypoxia hot spots, located at the front of the Yangtze River subaqueous delta adjacent to a submarine canyon, are at the conjunction between surface river plume and bottom saltwater intrusion (Fig. 1). Climate affects hypoxia in the region by controlling the physical stratification

<sup>1</sup>School of Geography and Ocean Science, Ministry of Education Key Laboratory for Coast and Island Development, Nanjing University, Nanjing 210023, China.

<sup>2</sup>State Key Laboratory of Estuarine and Coastal Research, School of Marine Sciences, East China Normal University, Shanghai 200241, China. <sup>3</sup>School of Geography and Environmental Science, University of Southampton, Southampton SO17 1BJ, UK. <sup>4</sup>CSDMS Integration Facility, INSTAAR, University of Colorado, Boulder, CO 80309-0545, USA. <sup>5</sup>Department of Geography, National University of Singapore, Singapore 117570, Singapore. <sup>6</sup>School of Marine Science and Engineering, Nanjing Normal University, Nanjing 210046, China. ✉e-mail: [nzhao@sklec.ecnu.edu.cn](mailto:nzhao@sklec.ecnu.edu.cn); [ypwang@nju.edu.cn](mailto:ypwang@nju.edu.cn)

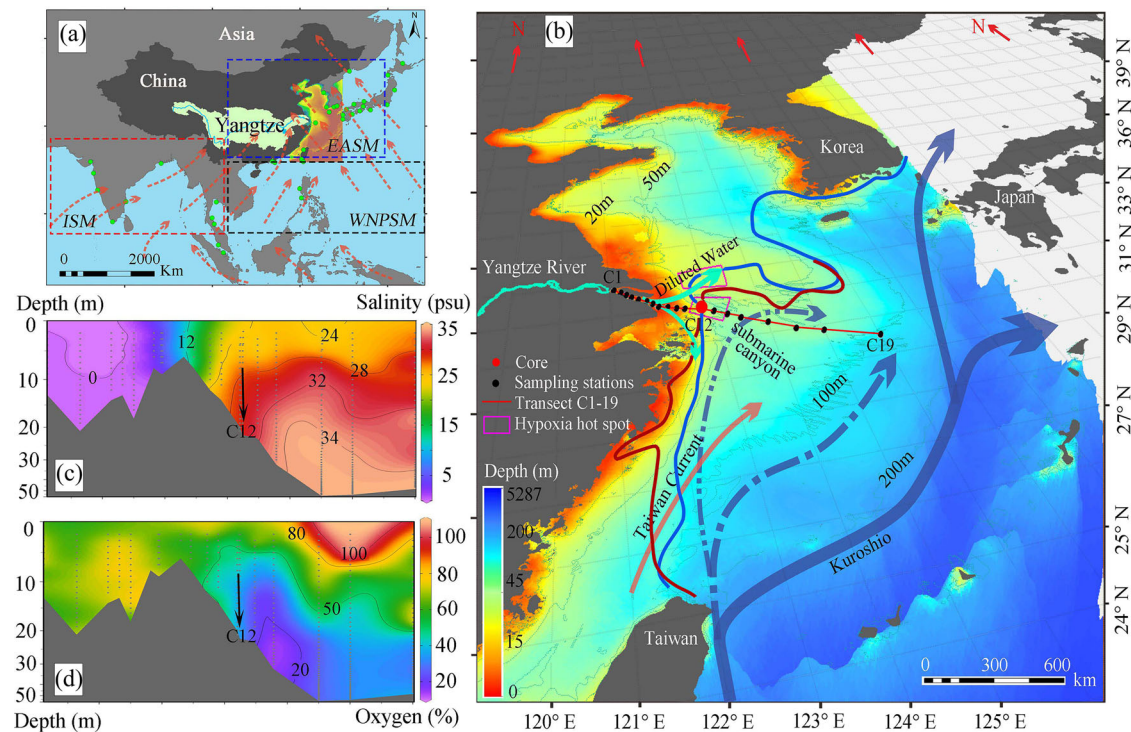


**Fig. 1 | The Yangtze River Basin, estuary and river-dominated shelf system.** **a** East Asian monsoon system: East Asian Summer Monsoon (EASM), Western North Pacific Summer Monsoon (WNPSM), and Indian Summer Monsoon (ISM). **b** Our study site (red dot) and the ocean current regime in the East China Sea: the dot dash and double dot dash blue lines with arrows represent the two main branches of the Kuroshio subsurface water intruding into the East China Sea shelf. The dark red and blue lines indicate the extent of bottom Kuroshio water intrusion in August and the annual average, respectively<sup>26,27</sup>. Bathymetric data are sourced from the ETOPO1 Global Relief Model (<https://www.ngdc.noaa.gov/mgg/global/etopo1sources.html>, last access: 22 March 2024). The salinity and dissolved oxygen saturation profiles along transect C1–19 are shown in (c) and (d), respectively, with our site situated near station C12. For detailed data source information, please refer to the “Methods” section. The maps were created using ArcScene 10.6 and OceanView 2.0 software.

generated by the vertical salinity gradients resulting from riverine freshwater discharge and (or) saltwater intrusion. On the other hand, human activities impact hypoxia in the region by altering nutrient levels. Specifically, the excessive use of chemical fertilizers in the basin has caused dissolved inorganic nitrogen (DIN) and phosphorus (DIP) to increase five-fold in the Yangtze Estuary<sup>19</sup>. Against the backdrop of drastic climate change and anthropogenic eutrophication in the Yangtze Estuary, it is important to understand whether the currently observed hypoxia is unprecedented, how to isolate the impacts of climate variability and human activities, as well as how hypoxia will evolve in the future.

To address these issues regarding hypoxia in the Yangtze Estuary, we collected a sediment core (Yt01; 122.74°E, 31.00°N, 25 m water depth) in 2018 using a drilling machine equipped with a hydraulic piston in the southern hot spot area where hypoxia occurs persistently<sup>17</sup> (Fig. 1). We obtained the history of hypoxia intensity and related driving factors over the past three centuries using sediment proxies and climate modeling results (see Methods). Specifically, we first reconstructed the variations in hypoxia intensity of the Yangtze Estuary by utilizing multiple redox sensitive trace elements (MultiRSTEs). Drawing upon the ecological preferences of sedimentary diatoms, we then reconstructed the salinity variations in both the surface and bottom layers of the Yangtze Estuary, from which we derived a proxy for vertical salinity gradient. This enabled us to estimate changes in the estuary’s stratification intensity over the past 300 years. Additionally, we derived the long-term nutrient variations in the Yangtze Estuary using diatom assemblages, elucidating the extent of eutrophication attributable to human activities. The watershed rainfall signal associated with large-scale climate variability plays a pivotal role in investigating how changes in the watershed affect the estuarine environment (e.g., salinity, nutrients and hypoxia). Therefore, we obtained the variations in the precipitation signal of the Yangtze Estuary over the past

300 years using the CESM model (<http://www.cesm.ucar.edu/models/cesm1.0/>), combined with hydrological and meteorological observational data. Our study provides insights that aid in delineating: (1) the historical variations of salinity, nutrients, and hypoxia in the Yangtze Estuary, (2) how climate variability influences these evolutions through land-sea interactions, and (3) the dominance of climate variability versus anthropogenic influences in the development and evolution of hypoxia in the Yangtze Estuary.

## Results and discussion

### Temporal variations in hypoxia intensity

Sensitive to the redox state of seawater, redox sensitive trace elements (RSTEs) have been widely used to discern anoxic and seasonally hypoxic conditions within silled, semi-silled basins, and estuaries<sup>20–22</sup>. The temporal variations of all RSTEs (V, Mo, Ni, As, Cr, Zn and Co) from our site show similar variations through the core even if they have different sensitivities to hypoxia (Fig. 2a). Therefore, we developed a dimensionless RSTEs index based on multiple elements to reconstruct long-term hypoxia conditions in the Yangtze Estuary (see Methods). Our results show that long-term variations of dissolved oxygen (DO) inferred from the MultiRSTEs index exhibit similar trends to those derived from foraminifera records ( $r = 0.66$ ,  $p < 0.05$ ) and instrumental observations, indicating adequate performance (Fig. 2b, c). The observed dissolved oxygen data are collected from various sampling stations across different seasons, whereas the reconstructed hypoxia data originates from a fixed site and may have chronological uncertainties. Consequently, there is a possibility of disparities between the observed and reconstructed data. However, when examined on decadal timescale, they demonstrate a notable level of consistency (Fig. 2b).

Overall, the intensity of hypoxia shows a decreasing trend (slope =  $-0.04$ ,  $p < 0.05$ ) during the period 1740–1975, with an increase

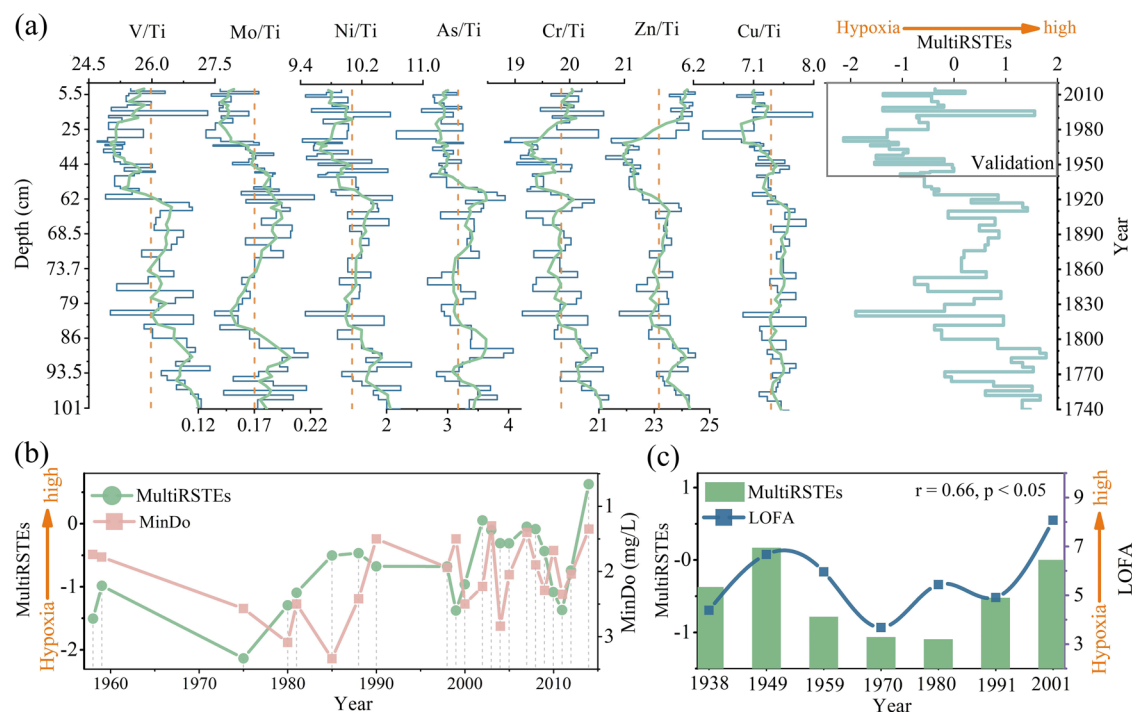


**Fig. 2 | Reconstruction and validation of hypoxia intensity in the Yangtze Estuary over the past three centuries.** **a** The depth profile of RSTE/Ti (ratio unit:  $10^{-3}$ ) is shown as a light blue line, while the green lines represent the five-point moving averages. The orange dot lines indicate the mean value of RSTE/Ti, and the gray rectangular box represents the validation period for the hypoxia reconstruction.

Comparative validations between the inferred hypoxia intensity from MultiRSTEs and **(b)** observations (minimum dissolved oxygen, MinDo) during 1958–2015, as well as **(c)** hypoxia intensity derived from low-oxygen foraminiferal assemblage (LOFA, Epistominella, Ammonia, Bulimina, Buliminella and Fursenkona) in period of 1938–2001<sup>40</sup>.

(slope = 0.15,  $p < 0.05$ ) afterwards (Fig. 2a). This recent period of enhanced hypoxia as inferred from the sedimentary record is consistent with observations, but importantly our results show that the intensity of hypoxia observed today does not reach the highest levels experienced in the last three centuries (Fig. 2a). The recent strong hypoxia condition is less severe than those experienced in the periods 1740–1800 and 1870–1920 (Fig. 2a).

### Hypoxia driving factors over the last three centuries

The formation and evolution of hypoxia in large river estuaries are strongly influenced by climate-driven physical stratification and human-induced eutrophication<sup>6,23</sup>. The strength of physical stratification in the Yangtze Estuary primarily depends on the vertical density gradient, which is governed by the dynamics of river plumes and the intrusion of saltwater from the bottom layers on the shelf<sup>24,25</sup>. Therefore, we use sedimentary diatoms, which are sensitive to environmental changes, as proxies to reconstruct long-term changes in surface and bottom salinity conditions, and to estimate the hypoxia-related physical stratification index and eutrophication (see “Methods” for details).

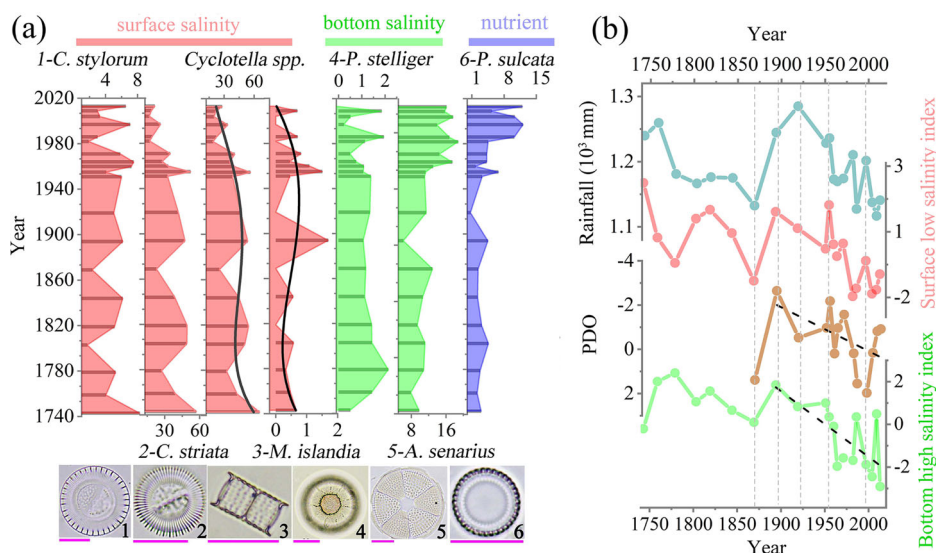
We identified 121 diatom species in 20 samples, including 58 centric species, 61 pennate species, a silicoflagellate species (*Dictyocha fibula*) and a diatom resting spores (see “Methods”). There are 15 diatom taxa with relative abundance larger than 1% (Supplementary Fig. S1). The communities are a combination of high-abundance (relative abundance >5%) brackish species (e.g., *Cyclotella striata*, *Cyclotella stylorum*) and marine species (e.g., *Paralia sulcata*, *Coscinodiscus radiatus*, *Actinopterychus senarius* and *Actinopterychus splendens*) and low-abundance (relative abundance <1%) freshwater species (*Melosira islandica*), which is consistent with the multiple water sources of various properties found in the Yangtze Estuary (i.e., the diluted Yangtze River water, the Kuroshio subsurface water intrusion and the Taiwan Current)<sup>26–28</sup>.

Based on previous studies and the response relationships between diatom abundance and salinity in the Yangtze Estuary (Supplementary

Fig. S2), we finally choose planktonic species *Cyclotella spp.* (*Cyclotella striata* and *Cyclotella stylorum*) and benthic species *Podosira stelliger* and *Actinopterychus senarius* as proxies to reconstruct variations in surface and bottom salinity conditions, respectively (Fig. 3a). Tychoplanktonic species *Paralia sulcata* are employed as a proxy for assessing long-term changes in nutrient conditions (Fig. 3a) (see “Methods” for details). Proxy results show that the surface water was in low-salinity conditions during the periods of 1775–1840 and 1890–1950, whereas relatively high-salinity conditions were predominantly found during 1975–2015 and the 1860s (Fig. 3b). The variations in surface salinity in the Yangtze Estuary are closely correlated with changes in river runoff into the sea. Our results show that the proxy-reconstructed variations of the surface low-salinity index are positively correlated ( $r = 0.62, p < 0.05$ ) with the rainfall signals generated by our climate model in the Yangtze River Basin over the last three centuries (Fig. 3b).

Reconstructed bottom high-salinity index has been decreasing (slope =  $-0.19, p < 0.05$ ) over the last 300 years, with higher salinities index in 1750–1950, the 1980s and 2010s (Fig. 3b). Previous studies have indicated that variations in the bottom salinity of the Yangtze Estuary are influenced by the intensity of Kuroshio Subsurface Water (KSSW) intrusion into the East China Sea<sup>27,28</sup>. Pacific Decadal Oscillation (PDO) exhibits a significant correlation ( $r = -0.63, p < 0.05$ ) with KSSW intrusion<sup>29</sup>. However, our findings demonstrate that the correlation ( $r = -0.33, p > 0.05$ ) between the bottom high-salinity index and PDO lacks statistical significance. Nonetheless, both variables exhibit similar long-term trends (Fig. 3b). Based on the surface and bottom water salinity indices, we further derived a stratification index of the Yangtze Estuary during 1740–2012 (see “Methods” for details). Our results reveal a decreasing trend (slope =  $-0.24, p < 0.05$ ) in the stratification strength of the Yangtze Estuary over the past three centuries, with a rapid decline after the 1950s (slope =  $-0.32, p < 0.05$ ) (Fig. 4a). The proxy-reconstructed nutrient level remained low with only modest changes during 1740–1975, however, they rapidly increased by a factor of 2.8 over the following half-century (Fig. 4c).

**Fig. 3 | Temporal variations of hypoxia driving factors over the last three centuries.** **a** Relative abundance (unit: %) of diatoms used for physical condition reconstructions: planktonic brackish species *Cyclotella* spp. including *Cyclotella stylorum* (*C. stylorum*) and *Cyclotella striata* (*C. striata*) and freshwater species *Melosira islandica* (*M. islandica*) serve as proxies for surface low-salinity conditions (red); benthic marine species *Podosira stelliger* (*P. stelliger*) and *Actinoptochus senarius* (*A. senarius*) act as proxies for bottom high-salinity conditions (green); tychoplanktonic marine species *Paralia sulcata* (*P. sulcata*) is a proxy for nutrient levels (purple). The black lines represent the polynomial fitting lines (polynomial order = 6). The six images at the bottom show microscopic photographs of the selected diatom species above (as noted by the numbers), and the pink scale lines indicate a length of 20  $\mu\text{m}$ . **b** Diatom-based surface and bottom salinity indices in the Yangtze Estuary, along with simulated precipitation in the Yangtze Basin and the changes in the Pacific Decadal Oscillation (PDO) (see “Methods”). The PDO data are sourced from <https://www.ncei.noaa.gov/pub/data/cmb/ersst> (last accessed on 10 October 2023). The black dashed lines represent the linear fitting trends for PDO and the bottom high-salinity index during 1890–2012, respectively.



### Evolution of hypoxia driving factors under land-sea interactions

Large-scale climate variability (e.g., PDO) modulate the variations in precipitation over the Yangtze Basin<sup>30,31</sup>. Rivers serve as a crucial link between land and sea, facilitating the conversion of basin precipitation into runoff and transmitting signals of climate variability to estuaries and coastal areas<sup>9</sup>. The enormous fluvial freshwater discharge influences the salinity and nutrient levels of the estuarine region<sup>24–26</sup>. Species-level changes in diatoms show a sensitive response to these environmental changes in the Yangtze Estuary<sup>19,32</sup>. Thus, it is plausible that signals of climate variability are imprinted on diatom population changes through riverine discharge and subsequently preserved in sediment records. Our results demonstrate a temporal similarity between the variations in model-simulated precipitation and the surface low-salinity index based on *Cyclotella* spp., with a significant positive correlation coefficient ( $r = 0.62$ ,  $p < 0.05$ ) (Fig. 3b). Moreover, the changes in PDO show a significant negative correlation ( $r = -0.64$ ,  $p < 0.05$ ) with the reconstructed surface low-salinity index (Fig. 3b). These significant correlations suggest a stable transmission relationship from large-scale climate variability (e.g., PDO) to watershed precipitation, fluvial discharge, estuarine surface salinity change and finally sedimentary diatom records over the last 300 years in the Yangtze system. The high sedimentation rate in estuaries enables the effective recording of environmental change signals at a high temporal resolution. Our findings also highlight the potential of using diatoms as a valuable tool to reconstruct high-resolution watershed environments and climate variability signals in estuarine settings.

Similar to the surface low-salinity index, we suggest that changes in the bottom high-salinity index are also linked to climate variability. Previous studies have indicated that the intrusion of high-salinity Kuroshio Sub-surface Water (KSSW) across the 200 m isobath in the East China Sea shelf region is a potential driving factor for bottom salinity changes in estuarine and shelf areas<sup>27,28</sup>, and that PDO has a significant negative correlation ( $r = -0.63$ ,  $p < 0.05$ ) with KSSW<sup>29</sup>. However, the main drivers of bottom salinity variations, including tides, waves, coastal currents, and offshore water masses and topography, vary depending on the timescales of interest<sup>27,33</sup>. Our data show that proxy-reconstructed bottom water salinity and PDO signals (closely related to KSSW) have no significant correlation

( $r = -0.33$ ,  $p > 0.05$ ) on interannual scale, but they show similar trends on longer time scale (Fig. 3b). Overall, climate variability has influenced the long-term evolution of surface and bottom salinity in the Yangtze Estuary, primarily through land-sea interactions. The vertical salinity gradient, in turn, has dominated the changes in physical stratification over the past three centuries.

Both climate variability and human activities have played pivotal roles in shaping the evolution of nutrients in the Yangtze Estuary. Prior to the widespread use of agricultural fertilizers in the basin, changes in estuarine nutrient levels were primarily influenced by climate-driven fluvial discharge. *Paralia sulcata*-based nutrient variations in the Yangtze Estuary during the period of 1740–1975 show consistent patterns with *Cyclotella* spp. and *Melosira islandica* which are closely related with fluvial freshwater discharge to the estuary (Fig. 3a). However, since 1975, human activities, specifically the extensive use of fertilizers, have become the primary controlling factor for the rapid and substantial increase in nutrient levels of the Yangtze Estuary (Fig. 4c). The nutrient level has rapidly increased by a factor of 2.8 over the following half-century (Fig. 4c).

### Climatic versus anthropogenic controls on hypoxia

Long-term and continuous observations of hypoxia in the Yangtze Estuary are deficient, and existing observational data has been influenced by human eutrophication, making it difficult to isolate the impacts of climate variability and human activities on estuarine hypoxia. By extending the reconstructions of hypoxia history and its key influencing factors to 300 years, we provided insights into the dominant driver(s) of the hypoxia evolution in the Yangtze Estuary from a longer-term perspective.

Our analysis indicates that climate variability modifies the stratification intensity of the estuary through land-sea interactions (riverine freshwater discharge and Kuroshio bottom intrusion), thereby controlling the evolution of hypoxia in the Yangtze Estuary during 1740–1975. We found a strong correlation ( $r = 0.72$ ,  $p < 0.05$ ) between a proxy-based stratification index and the reconstructed hypoxia intensity before 1975, when human activities had a minor impact and nutrient levels in the estuary were relatively low and stable (Fig. 4a–c). With the extensive use of agricultural fertilizers in the basin, nutrient levels in the estuary have

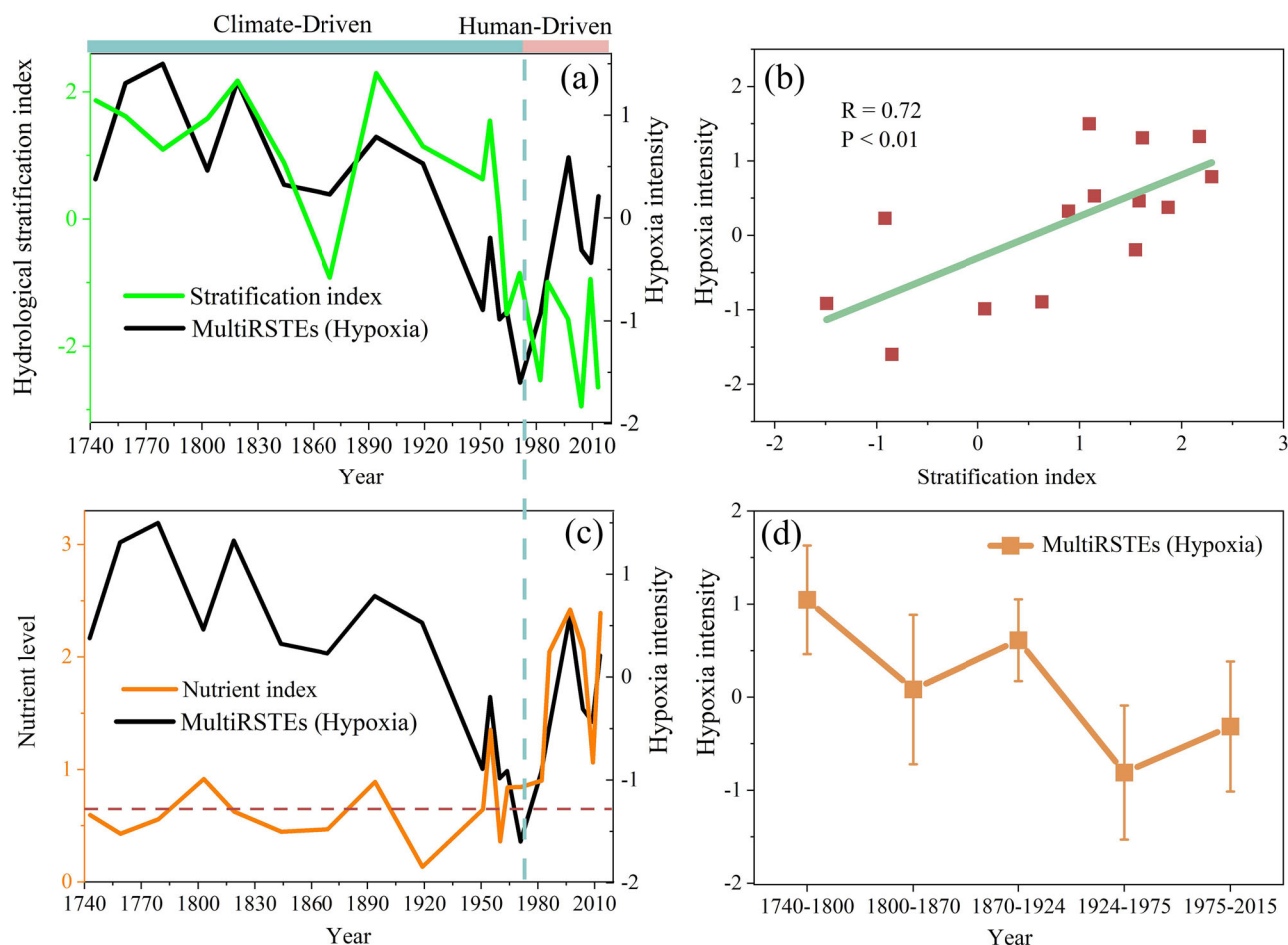


**Fig. 4 | The relationships between hypoxia and its main driving factors.** **a** Comparison between reconstructed hypoxia and stratification intensity indices over the past three hundred years. **b** The relationship between hypoxia and stratification intensity indices during 1740–1975. **c** Comparison of reconstructed hypoxia and estuarine nutrient levels, with the blue dashed line representing

when extensive usage of agricultural fertilizers started in the Yangtze Basin, and the dashed dark red line representing the nutrient baseline during 1740–1975. **d** The hypoxia intensity of the Yangtze Estuary during characteristic periods derived from MultiRSTEs, the error bar refers to the standard deviation of MultiRSTEs for each period.

rapidly increased (Fig. 4c), and human-induced eutrophication has dominated the evolution of hypoxia in the Yangtze Estuary. Our results indicate that the changes in hypoxia are consistent with the variations in nutrient levels since 1975 (Fig. 4c). However, despite the increase in hypoxia intensity of the Yangtze Estuary after 1975 due to human-induced eutrophication, the hypoxia intensity during this period remained lower than those of 1740–1800 and 1870–1924 (Fig. 4d). Our findings suggest that the hypoxia of the Yangtze Estuary in the recent decades was probably less developed than some preindustrial periods, primarily due to weaker physical stratification.

Similar to the Yangtze Estuary, the Mississippi Estuary was another example of large river-dominated estuarine systems that also experience seasonal hypoxia prior to human influences<sup>6,34</sup>. It is shown that although human-induced eutrophication has exacerbated hypoxia, the current observed hypoxia in the Mississippi Estuary is not the worst over the last 500 years<sup>34</sup> (Supplementary Fig. S3). Prior to human-induced eutrophication, a stable positive correlation ( $r = 0.58$ ,  $p < 0.05$ ) existed between hypoxia (based on low-oxygen tolerant benthic foraminifer proxy) and climate-driven fluvial discharge (reconstructed by floodwater sediments grain size in floodplain lakes)<sup>34–36</sup> (Supplementary Fig. S3). The histories of hypoxia in the two large estuaries highlight the pivotal role of climate variability in hypoxia development and its importance for predicting hypoxia in the world’s large estuarine systems. In the future, the key drivers of hypoxia may coincide in a manner that has not been experienced during the Anthropocene. Specifically, for the Yangtze Estuary, if

human activities continue to maintain high levels of nutrient supply to the estuary and climate-driven physical stratification strengthens, then there is a high risk that hypoxia in this large estuary may rise to unprecedented levels.

## Methods

### Chronology and grain size analysis

After getting dried and powdered, 25 samples sliced from the core (0–130 cm) with 1-cm thickness were sealed in a plastic box for 1 month to reach radioactive equilibrium. Then, the <sup>210</sup>Pb and <sup>137</sup>Cs activities for each sample were measured by HPGe  $\gamma$ -ray detector (Canberra Be3830). At ~60 cm, the <sup>210</sup>Pb activity reached a natural background level. In order to develop a longer age model, we prepared four optically stimulated luminescence (OSL) samples in a darkroom, and obtained enriched fine-grained quartz in each sample after removing carbonate and organic materials, separating fine-grained fraction and soaking in 40% hydrofluorosilicic acid. Luminescence measurements were conducted with Risø TL/OSL-DA-20C/D, and the equivalent dose (De) was calculated by the standard five-point single aliquot regeneration (SAR) method as described in ref. 37. The dose rate for OSL samples was determined by ICP-OES (K) and ICP-MS (U and Th). Finally, the age model of the Yt01 core (0–240 cm) was developed using Bacon (Version 2.3.9.1) based on <sup>210</sup>Pb, <sup>137</sup>Cs, and optically stimulated luminescence (OSL) data<sup>38</sup>. The detailed chronological results are shown in the supplementary information (Supplementary Note 1 and Fig. S4).

Grain size were analyzed using a Malvern Mastersizer 2000 at 2 cm intervals. Relevant analyses including the determination of grain size distribution curves, sand, silt, and clay content and mean, sorting, skewness, and kurtosis grain size parameters (Folk and Ward graphical measures) were conducted using GRADISTAT<sup>39</sup>. The results of grain size analysis indicate that the sedimentary environment of the site is characterized by weak hydrodynamics, which is typical of shallow marine and river sedimentary environments. Additionally, the results suggest that the sedimentary dynamics of the site are stable. Stable sedimentary environments are conducive to the preservation of sediment signals (such as sedimentary diatoms), providing suitable conditions for investigating variations in hypoxia and their responses to watershed environmental changes from a sedimentological perspective. The detailed results of grain size analysis are shown in the supplementary Information (Supplementary Note S3 and Fig. S5).

### Redox sensitive trace elements (RSTEs)

RSTEs are one of the most effective indicators used to reconstruct the long-term redox state of the sediment-water interface<sup>20–22</sup>. The abundance of RSTEs in sediments is strongly impacted by the oxidation level of the bottom water, and their enrichment is obvious in areas with hypoxia<sup>20–22</sup>. For example, using RSTEs, previous studies reported increasing hypoxia trends over the last few decades in the Yangtze Estuary, which are consistent with cruise observations and/or foraminiferal records<sup>18,40,41</sup>. In order to reconstruct long-term variations of DO content in this region, the depth profiles of RSTEs (V, Mo, Ni, As, Cr, Zn, Cu, U) were measured at 1-cm contiguous intervals using ICP-MS (Agilent 7700x) after digestion. The analytical precisions of trace elements with solid concentrations >10 ppm and >50 ppm are better than ±10% and ±5%, respectively.

The applicability of RSTEs to reconstruct DO is complicated by the input of terrestrial detritus<sup>20–22,42</sup>. Ti is mainly supplied from terrigenous clastics, so it is used as a normalizer (RSTE/Ti) to eliminate the impacts of terrestrial input changes in this study<sup>43</sup>. Previous studies have indicated that the distribution of some RSTEs (V, Mo, Ni and Cu) exhibit a response to the hypoxic conditions in the bottom water of the Yangtze Estuary<sup>41</sup>. However, unlike V, Mo, Ni and Cu, which are minimally affected by grain size effects, the distribution of U shows a high correlation (>0.7) with grain size in the Yangtze Estuary<sup>41</sup>. Therefore, although U is highly sensitive to redox environments and widely used to reconstruct redox conditions, it is not suitable for reconstructing changes in hypoxia in the Yangtze Estuary. Our data also show that, except for U, the temporal fluctuations of all RSTEs show similar patterns, even though they may have distinct sensitivities to hypoxia (Supplementary Fig. S6).

We reconstructed vertical variations of DO through the core based on selected multi RSTEs (V, Mo, Ni, As, Cr, Zn, Cu) data and a multi-proxy dimensionless method. Each applicable element is first made dimensionless according to Eq. (1):

$$\left(\frac{\text{RSTE}}{\text{Ti}}\right)^* = \frac{\text{RSTE}/\text{Ti} - \text{Mean}(\text{RSTE}/\text{Ti})}{\text{Stdev}(\text{RSTE}/\text{Ti})} \quad (1)$$

where RSTE/Ti is the abundance of each element normalized by that of Ti in a given sample, and (RSTE/Ti)\* is the corresponding dimensionless value; Mean(RSTE/Ti) is the mean value of all samples for each element and Stdev(RSTE/Ti) is the associated standard deviation.

The resulting dimensionless RSTEs are then averaged to obtain the MultiRSTEs index. This implies that each selected redox element carries equal weight in the DO reconstruction. Finally, the reconstructed DO changes were validated by benthic foraminiferal records and observations of hypoxia in this region.

### Sedimentary diatom analysis

Diatoms are widely used in paleoenvironmental reconstructions due to their abundance in marine, brackish, and freshwater environments, as well as their sensitivity to environmental changes<sup>44,45</sup>. Previous studies have shown

that the evolution of hypoxia is closely related to changes in water stratification and nutrient levels<sup>6,7,23</sup>. In this study, sedimentary diatoms preserved in the core were employed as proxies to reconstruct the fluctuations of salinity conditions in both the surface and bottom layers of the Yangtze Estuary, and further estimate the intensity of physical stratification by reconstructing the salinity difference between the surface and bottom layers. Additionally, long-term changes in the nutrient level of the estuary was also derived from representative diatom species.

The uppermost meter of the core was sampled at 5-cm intervals and processed using the following protocol to obtain slides of sedimentary diatoms<sup>46</sup>. Specifically, all samples were first freeze-dried, and then processed by a standard chemical pre-treatment to remove carbonate (10% hydrochloric acid), organic matter (30% hydrogen peroxide) and clay (ammonium hydroxide solution). After chemical treatment, the samples were floated with a heavy liquid of zinc bromide at a specific gravity of 2.4 to separate siliceous fractions. Finally, 0.1 ml diluted suspension was transferred to the coverslips to make slides. We counted all the diatom valves under an Olympus CX-31 light microscope at a magnification of ×1000. The total number of diatom valves counted in most samples exceeds 300. Diatoms were identified to species level using historical literatures<sup>47–49</sup>, and classified by salinity based on “Algae Database” (<http://www.algaebase.org>, accessed October, 2023) into freshwater, brackish and marine species. We calculated the abundance of each taxon by determining its percentage relative to the total count of diatom frustules. Considering the potential errors in identification and statistical analysis, we selected species with abundance greater than 1% as potential proxies for reconstructing salinity and nutrient levels<sup>50</sup>. In addition, rare species with abundance lower than 1%, but with meaningful indicative value for environmental variables, were used as supplementary indicators to further validate the selected proxies.

### Diatom proxies for physical conditions and nutrient level

The salinity in the Yangtze Estuary exhibits spatiotemporal fluctuations (19–33.5 psu) due to the changes in fluvial freshwater input and intrusion of saltwater from the East China Sea<sup>51</sup>. Observational data also show that the vertical salinity at station C12 gradually increases from 22.0 psu in the surface layer to 31.5 psu in the bottom layer, demonstrating a notable salinity gradient (Fig. 1c). Based on the ecological habits of diatoms and previous studies in the Yangtze Estuary and adjacent waters, we classified the identified high-abundance diatoms into planktonic, benthic and tychoplanktonic groups<sup>47–49</sup>. And then, we analyzed the relationship between planktonic species abundance and surface salinity, as well as benthic species abundance and bottom salinity, to identify appropriate diatom assemblages for reconstructing salinity conditions (Supplementary Figs. S2 and S7).

Specifically, *Cyclotella* spp. (*Cyclotella striata* and *Cyclotella stylorum*) are planktonic brackish species. Prior studies have elucidated the potential of *Cyclotella* spp. as a salinity proxy, due to its discernible negative associations with both salinity and water depth<sup>19,52,53</sup>. Notably, *Cyclotella* spp. have been extensively employed as an indicator for nearshore low-salinity environments that undergo discernible influences from freshwater inputs<sup>54,55</sup>. We found a significant negative correlation ( $r = -0.55$ ,  $p < 0.05$ ) between the abundance of *Cyclotella* spp. (*Cyclotella striata* and *Cyclotella stylorum*) and surface salinity in the Yangtze Estuary (Supplementary Fig. S2a, d). Based on prior studies and the relationship between *Cyclotella* spp. and surface salinity, we selected *Cyclotella* spp. as a proxy for reconstructing surface salinity condition in this region.

The abundance of *Coscinodiscus radiatus* (planktonic marine species) and *Cyclotella* spp. (planktonic brackish species) in the core exhibit consistently opposing temporal variations (Supplementary Fig. S1). However, there is no statistically significant correlation ( $p > 0.05$ ) between the spatial variations in the abundance of *Coscinodiscus radiatus* and surface salinity within the Yangtze Estuary. Therefore, Planktonic *Coscinodiscus radiatus* was not used as a proxy for reconstructing surface salinity variations in this study. *Melosira islandica*, a freshwater species,

serves as an potential indicator of the intensity of fluvial freshwater impact in the study area<sup>56,57</sup>. However, due to its relative abundance of less than 1%, its robustness as an indicator of surface salinity is limited. Nevertheless, it can be employed as a supplementary proxy to validate the reconstructed changes in surface salinity. Our findings demonstrate that the abundance variations of *Melosira islandica* in the core generally align with those of *Cyclotella spp.*, reaffirming the effectiveness of *Cyclotella spp.* as a proxy of surface salinity (Fig. 3a).

*Podosira stelliger*, a benthic marine diatom, has been found to exhibit a significant correlation with salinity<sup>32,58,59</sup>. For example, a study investigated seawater intrusion during storm surges by leveraging the relationship between *Podosira stelliger* and salinity, as well as its benthic ecological characteristics<sup>59</sup>. *Podosira stelliger* is highly responsive to bottom salinity, displaying a positive correlation with water depth and salinity in China's eastern continental shelf<sup>32</sup>. We also found a significant positive correlation ( $r = 0.55$ ,  $p < 0.05$ ) between the abundance of *Podosira stelliger* and bottom salinity in the Yangtze Estuary (Supplementary Fig. S2b, d). Additionally, when salinity drops below 32 psu, there is a notable decrease in its abundance<sup>32</sup>. The salinity in the hypoxic hotspot area (C12–C14) fluctuates between 22.0–34.6 psu, with the bottom salinity ranging from 28.6 to 34.6 psu (Fig. 1c). The boundary where the abundance of *Podosira stelliger* undergoes rapid changes falls around 32 psu. Therefore, we selected *Podosira stelliger* as a proxy for reconstructing bottom salinity in this region. However, although *Podosira stelliger* is sensitive to salinity, it also prefers high-temperature environments<sup>32,58,59</sup>. Therefore, during periods of temperature increase, the reconstructed bottom high-salinity index based on *Podosira stelliger* may be biased toward higher values.

*Actinopterychus splendens* is a benthic marine species that predominantly inhabits nearshore environments with higher salinity levels and a broad temperature range<sup>60</sup>. Our results reveal a notable increase in the abundance of this species with water depth and salinity in the Yangtze Estuary (Supplementary Fig. S7). However, no significant correlation ( $r = 0.01$ ,  $p > 0.05$ ) was observed between its abundance and bottom salinity. *Actinocyclus ehrenbergii* and *Actinopterychus senarius* are nearshore benthic marine species with high abundance in low-salinity waters<sup>32,53,61</sup>. They can serve as proxies for salinity and sea level<sup>53,61</sup>. Our results indicate that the abundances of both *Actinopterychus senarius* and *Actinocyclus ehrenbergii* decrease with increasing water depth and salinity in the Yangtze Estuary (Supplementary Figs. S2c and S7). However, only the abundance of *Actinopterychus senarius* shows a significant correlation ( $r = -0.55$ ,  $p < 0.05$ ) with bottom salinity (Supplementary Fig. S2d). The *Actinocyclus ehrenbergii* has a weak correlation ( $r = -0.34$ ,  $p > 0.05$ ) with bottom salinity because of its susceptibility to temperature (it thrives in low-temperature environments<sup>61</sup>). Based on previous studies and the relationships between benthic diatom species and bottom salinity in the Yangtze Estuary, we ultimately identified *Podosira stelliger* and *Actinopterychus senarius* as good candidates for establishing the bottom salinity index in this region.

*Paralia sulcata*, a tycho planktonic marine species, demonstrates a broad salinity tolerance, ranging from 5 to 35 psu. However, its optimal range for survival typically falls between 25 and 35 psu<sup>48,62,63</sup>. The salinity fluctuations observed within the study region, ranging from 22 to 34.6 psu, closely align with this optimal range. Thus, it can be inferred that salinity, despite exhibiting spatiotemporal variations in this region, does not exert a dominant influence on *Paralia sulcata* abundance. Furthermore, several studies have revealed a positive correlation between the high abundance of *Paralia sulcata* and nutrient levels<sup>32,63</sup>. *Paralia sulcata* was also used as a potential indicator of nutrient-rich upwelling areas<sup>64</sup>. The abundance of *Paralia sulcata* in sediments has been found to be significantly correlated with the concentration of nitrogen and phosphorus in the upper water column of East China Sea<sup>32,65</sup>. Consequently, *Paralia sulcata* was selected as a proxy for assessing nutrient levels in this study. It is noteworthy that while the optimal ecological niche of *Paralia sulcata* aligns with the salinity range of the Yangtze Estuary, thereby diminishing the impact of salinity on *Paralia*

*sulcata* abundance, temperature emerges as a potential confounding factor. As temperature rises, the growth of *Paralia sulcata* becomes suppressed<sup>62,63</sup>. Consequently, during periods characterized by temperature increases, the nutrient levels inferred from *Paralia sulcata* may underestimate the actual situation.

After identifying diatom species for reconstructing physical conditions, we performed a normalization to the abundance of *Cyclotella spp.* (similar as Eq. (1)) and derived a surface low-salinity index (Fig. 3). To avoid potential bias caused by high-abundance species overshadowing low-abundance species during the reconstruction of bottom salinity condition, we did not directly sum the abundances of *Actinopterychus senarius* (with a mean relative abundance of 12.8%) and *Podosira stelliger* (with a mean relative abundance of 1.1%) (Supplementary Fig. S1). Instead, we normalized both species and summed the negative value of normalized *Actinopterychus senarius* (negatively associated with bottom salinity) with the value of normalized *Podosira stelliger* (positively associated with bottom salinity) to derive a bottom high-salinity index (Fig. 3). We estimated the relative changes in nutrient levels by calculating the ratio between the abundance of *Paralia sulcata* and its mean during 1740–2015 (Figs. 3a and 4c).

Salinity-induced density gradients have been identified as the primary driver of stratification intensity in the Yangtze Estuary. When surface low-salinity conditions coexist with bottom high-salinity conditions, a vertical density gradient is established, leading to pronounced physical stratification within the water column. Therefore, we derive a stratification intensity index using the reconstructed surface and bottom salinity indices. To avoid excessive weighting of the bottom salinity, we first normalized the bottom high-salinity index, which was calculated from two components (see above). Then, we added up the normalized bottom high-salinity index and the surface low-salinity index to obtain a stratification intensity index (Fig. 4a).

### Long-term climate data in the Yangtze River Basin

We employed a climate model in combination with observational meteorological data and historical hydrological gauging records from the Datong station to reconstruct the precipitation history for the Yangtze Basin from 1740 to 2012 (Supplementary Note 3 and Fig. S8). We simulated rainfall amount (at about  $3.75^\circ \times 3.75^\circ$  spatial resolution) during 1740–2000 in the Yangtze Basin with the fully-coupled earth system model CESM (<http://www.cesm.ucar.edu/models/cesm1.0/>). The observational rainfall data for the Yangtze Basin during 1955–2012 were obtained from the National Meteorological Data Center (<http://data.cma.cn>). We also obtained gauging hydrological data at Datong Station (which effectively monitored the Yangtze River's freshwater discharge into the coastal ocean) during 1890–2012 from the China Hydrological Statistical Yearbook. The historical hydrological data were converted into precipitation based on the relationship between measured basin precipitation and runoff during 1955–2012 (Supplementary Fig. S8b). We obtained a comprehensive precipitation dataset spanning from 1740 to 2012 by performing data assimilation on three different rainfall data sources from meteorological stations, hydrological-meteorological relationships and modeling outputs. The simulated data and observed data are both available for the period during 1955–2000. Therefore, we selected the data from this period as the analysis sample to assimilate the whole simulated time series (1740–2000). During the period from 1955 to 2000, we performed a regression analysis on both observed and simulated data after sorting. Then, we applied self-adjusting multi-order fitting techniques to correct the whole series of simulated climate data using Matlab (version R2019b). This assimilation method ensures that the amplitude of simulated results corresponds to the observed scale while maintaining the phase of climate oscillations over time. As a result, it preserves the temporal variation of model outputs. Finally, based on the principle of prioritizing observational data, the final dataset for precipitation in the Yangtze Basin during 1740–2012 is constructed by combining meteorological observations from 1952 to 2012, hydro-meteorological calculated data from 1890 to 1955, and assimilated simulated data from 1740 to 1890.

The rainfall signal serves as a vital link for analyzing whether climate variability signals can be preserved in sedimentary records through land-sea interactions. It is also a key environmental factor for investigating the impacts of watershed environmental changes on estuarine and coastal regions. When comparing the estuarine sediment diatom data with the watershed precipitation signal, it is necessary to conduct the analysis on a consistent time scale. The diatom frustules in every 2-cm sample were counted, which roughly corresponds to a 5-year averaging value (sedimentation rate of ~0.36 cm/year). Therefore, we performed a 5-year moving averaging on the obtained annual watershed precipitation data during 1740–2015 to achieve a similar resolution for comparison with the diatom data.

### Marine observational data

The observational salinity and DO data in Fig. 1 were from the Comprehensive Scientific Expedition on the East China Sea Shelf conducted by Tongji University in September 2019. We obtained salinity profiles using a Sea-Bird 911 plus CTD instrument and collected six-layer seawater samples at each station using Niskin bottles. DO was measured using both polarographic and traditional Winkler titration methods<sup>66</sup>. We employed the simple Kriging interpolation method to obtain profiles of salinity and dissolved oxygen (Fig. 1).

The salinity data for the surface and bottom layers in Fig. S2 were obtained from the “Evolution of the Yangtze River Frontal Structure and Its Response to Land-Sea Condition Variations” project in October 2023, which was part of the Shiptime Sharing Project of National Natural Science Foundation of China. The sampling region spanned 29.5°N, 121.1°E to 32.5°N, 124.0°E, including 9 sections and 64 sampling stations. Salinity profile data were measured using the Sea-Bird 911 plus CTD instrument, and we utilized the simple Kriging interpolation method to obtain the spatial distribution of surface and bottom salinity in the Yangtze Estuary (Supplementary Figs. S2 and S7).

### Data availability

All data compiled and analyzed in this study are publicly available at <https://doi.org/10.6084/m9.figshare.25604007>.

Received: 7 June 2023; Accepted: 19 April 2024;

Published online: 04 May 2024

### References

- Breitburg, D. et al. Declining oxygen in the global ocean and coastal waters. *Science* **359**, eaam7240 (2018).
- Diaz, R. J. & Rosenberg, R. Spreading dead zones and consequences for marine ecosystems. *Science* **321**, 926–929 (2008).
- Best, J. Anthropogenic stresses on the world’s big rivers. *Nat. Geosci.* **12**, 7–21 (2019).
- Breitburg, D. L., Hondorp, D. W., Davias, L. A. & Diaz, R. J. Hypoxia, nitrogen, and fisheries: integrating effects across local and global landscapes. *Annu. Rev. Mar. Sci.* **1**, 329–349 (2009).
- Rabalais, N. N. & Turner, R. E. Gulf of Mexico hypoxia: past, present, and future. *Limnol. Oceanogr. Bull.* **28**, 117–124 (2019).
- Fennel, K. & Testa, J. M. Biogeochemical controls on coastal hypoxia. *Annu. Rev. Mar. Sci.* **11**, 105–130 (2019).
- Rabalais, N. et al. Dynamics and distribution of natural and human-caused hypoxia. *Biogeosciences* **7**, 585–619 (2010).
- Izett, J. G. & Fennel, K. Estimating the cross-shelf export of riverine materials: Part 2. Estimates of global freshwater and nutrient export. *Glob. Biogeochem. Cycles* **32**, 176–186 (2018).
- Milliman, J. D. & Farnsworth, K. L. *River Discharge to the Coastal Ocean: A Global Synthesis* (Cambridge University Press, 2011).
- Claret, M. et al. Rapid coastal deoxygenation due to ocean circulation shift in the northwest Atlantic. *Nat. Clim. Change* **8**, 868–872 (2018).
- Jutras, M., Dufour, C., Mucci, A., Cyr, F. & Gilbert, D. Temporal changes in the causes of the observed oxygen decline in the St. Lawrence Estuary. *J. Geophys. Res. Oceans* **125**, e2020JC016577 (2020).
- Gilbert, D., Rabalais, N., Diaz, R. & Zhang, J. Evidence for greater oxygen decline rates in the coastal ocean than in the open ocean. *Biogeosciences* **7**, 2283–2296 (2010).
- Levin, L. et al. Effects of natural and human-induced hypoxia on coastal benthos. *Biogeosciences* **6**, 2063–2098 (2009).
- Jokinen, S. A. et al. A 1500-year multiproxy record of coastal hypoxia from the northern Baltic Sea indicates unprecedented deoxygenation over the 20th century. *Biogeosciences* **15**, 3975–4001 (2018).
- Altieri, A. H. & Gedan, K. B. Climate change and dead zones. *Glob. Change Biol.* **21**, 1395–1406 (2015).
- Wang, F., Liu, J., Qiu, J. & Wang, H. Historical evolution of hypoxia in the East China Sea off the Changjiang (Yangtze River) estuary for the last ~13,000 years: evidence from the benthic foraminiferal community. *Cont. Shelf Res.* **90**, 151–162 (2014).
- Zhang, W., Wu, H., Hetland, R. D. & Zhu, Z. On mechanisms controlling the seasonal hypoxia hot spots off the Changjiang River Estuary. *J. Geophys. Res. Oceans* **124**, 8683–8700 (2019).
- Wu, Y., Fan, D., Wang, D. & Yin, P. Increasing hypoxia in the Changjiang Estuary during the last three decades deciphered from sedimentary redox-sensitive elements. *Mar. Geol.* **419**, 106044 (2020).
- Wang, Y., Xu, H. & Li, M. Long-term changes in phytoplankton communities in China’s Yangtze Estuary driven by altered riverine fluxes and rising sea surface temperature. *Geomorphology* **376**, 107566 (2021).
- Algeo, T. J. & Li, C. Redox classification and calibration of redox thresholds in sedimentary systems. *Geochim. Cosmochim. Acta* **287**, 8–26 (2020).
- Algeo, T. J. & Liu, J. A re-assessment of elemental proxies for paleoredox analysis. *Chem. Geol.* **540**, 119549 (2020).
- Bennett, W. W. & Canfield, D. E. Redox-sensitive trace metals as paleoredox proxies: a review and analysis of data from modern sediments. *Earth Sci. Rev.* **204**, 103175 (2020).
- Goody, A. et al. Historical records of coastal eutrophication-induced hypoxia. *Biogeosciences* **6**, 1707–1745 (2009).
- Geyer, W. R. & MacCready, P. The estuarine circulation. *Annu. Rev. Fluid Mech.* **46**, 175–197 (2014).
- Wu, H., Zhu, J., Shen, J. & Wang, H. Tidal modulation on the Changjiang River plume in summer. *J. Geophys. Res. Oceans* **116**, C08017 (2011).
- Wu, R., Wu, H. & Wang, Y. Modulation of shelf circulations under multiple river discharges in the East China Sea. *J. Geophys. Res. Oceans* **126**, e2020JC016990 (2021).
- Xu, L., Yang, D., Benthuyzen, J. A. & Yin, B. Key dynamical factors driving the Kuroshio subsurface water to reach the Zhejiang coastal area. *J. Geophys. Res. Oceans* **123**, 9061–9081 (2018).
- Yang, D. et al. Numerical study on the pattern and origins of Kuroshio branches in the bottom water of southern East China Sea in summer. *J. Geophys. Res. Oceans* **117**, C02014 (2012).
- Yang, D. et al. Numerical study on inter-annual variation of cross-shelf intrusion of Kuroshio into East China Sea. *Oceanol. Limnol. Sin.* **48**, 1318–1327 (2017).
- Wang, M. et al. Precipitation in eastern China over the past millennium varied with large-scale climate patterns. *Commun. Earth Environ.* **3**, 321 (2022).
- Wu, M., Rong-Hua, Z., Hu, J. & Zhi, H. Synergistic interdecadal evolution of precipitation over Eastern China and the Pacific decadal oscillation during 1951–2015. *Adv. Atmos. Sci.* **41**, 53–72 (2023).
- Wang, Y., Liu, D., Di, B., Shi, Y. & Wang, Y. Distribution of diatoms and silicoflagellates in surface sediments of the Yellow Sea and offshore from the Changjiang River, China. *Chin. J. Oceanol. Limnol.* **34**, 44–58 (2016).



33. Zhu, J., Wu, H., Li, L. & Qiu, C. Saltwater intrusion in the Changjiang Estuary. In *Coastal environment, disaster, and infrastructure - A case study of China's coastline* (eds Liang, X. S. & Zhang, Y.) 49–73 (2018). IntechOpen <https://doi.org/10.5772/intechopen.80903>.
34. Swarzenski, P., Campbell, P., Osterman, L. & Poore, R. A 1000-year sediment record of recurring hypoxia off the Mississippi River: the potential role of terrestrially-derived organic matter inputs. *Mar. Chem.* **109**, 130–142 (2008).
35. Munoz, S. E. et al. Cahokia's emergence and decline coincided with shifts of flood frequency on the Mississippi River. *Proc. Natl Acad. Sci.* **112**, 6319–6324 (2015).
36. Osterman, L., Campbell, P., Swarzenski, P. & Ricardo, J. *Biological, Physical and Geochemical Data from Gulf of Mexico Core MRJ0504*. US Geological Survey Open File Report 1024 (2007).
37. Murray, A. S. & Wintle, A. G. Luminescence dating of quartz using an improved single-aliquot regenerative-dose protocol. *Radiat. Meas.* **32**, 57–73 (2000).
38. Blaauw, M. & Christen, J. A. Flexible paleoclimate age–depth models using an autoregressive gamma process. *Bayesian Anal.* **6**, 457–474 (2011).
39. Blott, S. J. & Pye, K. GRADISTAT: a grain size distribution and statistics package for the analysis of unconsolidated sediments. *Earth Surf. Process. Landf.* **26**, 1237–1248 (2001).
40. Li, X. et al. Historical trends of hypoxia in Changjiang River estuary: applications of chemical biomarkers and microfossils. *J. Mar. Syst.* **86**, 57–68 (2011).
41. Xu, S., Zhai, S., Zhang, A., Zhang, H. & Lu, H. Redox environment effect on redox sensitive elements in surface sediments of the Changjiang Estuary hypoxia zone. *Front. Earth Sci. China* **2**, 10–16 (2008).
42. Morford, J. L. & Emerson, S. The geochemistry of redox sensitive trace metals in sediments. *Geochim. Cosmochim. Acta* **63**, 1735–1750 (1999).
43. Tribouillard, N., Algeo, T. J., Lyons, T. & Riboulleau, A. Trace metals as paleoredox and paleoproductivity proxies: an update. *Chem. Geol.* **232**, 12–32 (2006).
44. Battarbee, R. et al. An information system for palaeoenvironmental reconstruction. *EDDI*. **81**, 1–94 (2001).
45. Smol, J. P. & Stoermer, E. F. *The Diatoms: Applications for the Environmental and Earth Sciences* (Cambridge University Press, 2010).
46. Renberg, I. A procedure for preparing large sets of diatom slides from sediment cores. *J. Paleolimnol.* **4**, 87–90 (1990).
47. Dexiang, J. *Marine Benthic Diatoms in China* 585–619 (China Ocean Press, 1992).
48. Hasle, G. R., Syvertsen, E. E., Steidinger, K. A., Tangen, K. & Tomas, C. R. *Identifying Marine Diatoms and Dinoflagellates* (Elsevier, 1996).
49. Yang, S. & Dong, S. *Common Planktonic Diatoms Atlas of Chinese Seas* (Ocean University of China Press, 2006).
50. Kato, K. Deletion of less-abundant species from ecological data. *Diatom* **8**, 1–5 (1993).
51. Chen, C.-T. A. Chemical and physical fronts in the Bohai, Yellow and East China seas. *J. Mar. Syst.* **78**, 394–410 (2009).
52. McQuoid, M. & Hobson, L. A Holocene record of diatom and silicoflagellate microfossils in sediments of Saanich Inlet, ODP Leg 169S. *Mar. Geol.* **174**, 111–123 (2001).
53. Mirabdullayev, I. M. et al. Succession of the ecosystems of the Aral Sea during its transition from oligohaline to polyhaline water body. *J. Mar. Syst.* **47**, 101–107 (2004).
54. Ta, T. K. O., Nguyen, V. L., Tateishi, M., Kobayashi, I. & Saito, Y. Sedimentary facies, diatom and foraminifer assemblages in a late Pleistocene–Holocene incised-valley sequence from the Mekong River Delta, Bentre Province, Southern Vietnam: the BT2 core. *J. Asian Earth Sci.* **20**, 83–94 (2001).
55. Zong, Y. et al. Diatoms from the Pearl River estuary, China and their suitability as water salinity indicators for coastal environments. *Mar. Micropaleontol.* **75**, 38–49 (2010).
56. Patrick, R. Ecology of freshwater diatoms and diatom communities. In *The biology of diatoms*, 284–326 (University of California Press, 1977).
57. Stoermer, E. F., Kreis, R. G. Jr & Andresen, N. A. Checklist of diatoms from the Laurentian Great Lakes. II. *J. Great Lakes Res.* **25**, 515–566 (1999).
58. Koc Karpuz, N. & Schrader, H. Surface sediment diatom distribution and Holocene paleotemperature variations in the Greenland, Iceland and Norwegian Sea. *Paleoceanography* **5**, 557–580 (1990).
59. Zong, Y. & Tooley, M. J. Evidence of mid-Holocene storm-surge deposits from Morecambe Bay, northwest England: a biostratigraphical approach. *Quat. Int.* **55**, 43–50 (1999).
60. Foged, N. Diatoms in eastern Australia. *Bibl. Phycol. Band* **41**, 243 (1978).
61. Rijstenbil, J. Phytoplankton composition of stagnant and tidal ecosystems in relation to salinity, nutrients, light and turbulence. *Neth. J. Sea Res.* **21**, 113–123 (1987).
62. McQuoid, M. R. & Nordberg, K. The diatom *Paralia sulcata* as an environmental indicator species in coastal sediments. *Estuar. Coast. Shelf Sci.* **56**, 339–354 (2003).
63. Zong, Y. Implications of *Paralia sulcata* abundance in Scottish isolation basins. *Diatom Res.* **12**, 125–150 (1997).
64. Abrantes, F. Diatom assemblages as upwelling indicators in surface sediments off Portugal. *Mar. Geol.* **85**, 15–39 (1988).
65. Di, B. et al. Diatom and silicoflagellate assemblages in modern surface sediments associated with human activity: a case study in Sishili Bay, China. *Ecol. Indic.* **24**, 23–30 (2013).
66. Bryan, J., Riley, J. & Williams, P. L. A Winkler procedure for making precise measurements of oxygen concentration for productivity and related studies. *J. Exp. Mar. Biol. Ecol.* **21**, 191–197 (1976).

## Acknowledgements

The financial support for this study was provided by the National Natural Science Foundation of China (NSFC) under grant numbers U2240220, 42030402, and 41625012, as well as by the Innovation Program of the Shanghai Municipal Education Commission (project number 2019-01-07-00-05-E00027). N.Z. acknowledges funding from Shanghai Pilot Program for Basic Research (grant number TQ20220101). Additionally, H.S. received funding from the NSFC Youth Project (grant number 42306098). Support for A.J.K. came from the US National Science Foundation (grant number 0621695). The hydrological data were collected onboard of R/V Ke Xue San (Bo Hai Ke or Chuang Xin Yi) implementing the open research cruise NORC2023-03 + NORC2023-302 supported by NSFC Shiptime Sharing Project (project number: 42249903). We are also thankful to Dr. Jian Liu for her valuable suggestions regarding the climate model. Dr. Yang Zhang and Mr. Chipeng He provided assistance with the geochemical and sedimentary diatom analyses. Our gratitude extends to the editor, Dr. Olivier Sulpis, and to Dr. Françoise Chalié, Dr. Rick Hennekam and an anonymous reviewer who provided constructive suggestions on the manuscript.

## Author contributions

Y.P.W. framed the study. H.S., Y.Z., N.Z., D.L., and S.E.D. conducted formal analysis. H.S., S.E.D., N.Z., X.L., A.J.K., Y.Y. and J.G. wrote the manuscript. All authors discussed and interpreted the results.

## Competing interests

The authors declare no competing interests. N.Z. is an Editorial Board Member for Communications Earth & Environment, but was not involved in the editorial review of, nor the decision to publish this article.

## Additional information

**Supplementary information** The online version contains supplementary material available at <https://doi.org/10.1038/s43247-024-01403-w>.

**Correspondence** and requests for materials should be addressed to Ning Zhao or Ya Ping Wang.

**Peer review information** *Communications Earth and Environment* thanks Rick Hennekam, Françoise Chalié and the other, anonymous, reviewer(s) for their contribution to the peer review of this work. Primary Handling Editors: Olivier Sulpis and Clare Davis. A peer review file is available.

**Reprints and permissions information** is available at <http://www.nature.com/reprints>

**Publisher's note** Springer Nature remains neutral with regard to jurisdictional claims in published maps and institutional affiliations.

**Open Access** This article is licensed under a Creative Commons Attribution 4.0 International License, which permits use, sharing, adaptation, distribution and reproduction in any medium or format, as long as you give appropriate credit to the original author(s) and the source, provide a link to the Creative Commons licence, and indicate if changes were made. The images or other third party material in this article are included in the article's Creative Commons licence, unless indicated otherwise in a credit line to the material. If material is not included in the article's Creative Commons licence and your intended use is not permitted by statutory regulation or exceeds the permitted use, you will need to obtain permission directly from the copyright holder. To view a copy of this licence, visit <http://creativecommons.org/licenses/by/4.0/>.

© The Author(s) 2024